

Examples of Design of Vacuum Systems for Accelerators JUAS 2013

Roberto Kersevan

Technology Department
Vacuum Surfaces and Coatings Group
CERN, CH-1211 Geneva

AGENDA:

1. Introduction
2. Analytical and numerical methods
3. Vacuum chamber geometries by examples
4. Conclusions
5. References

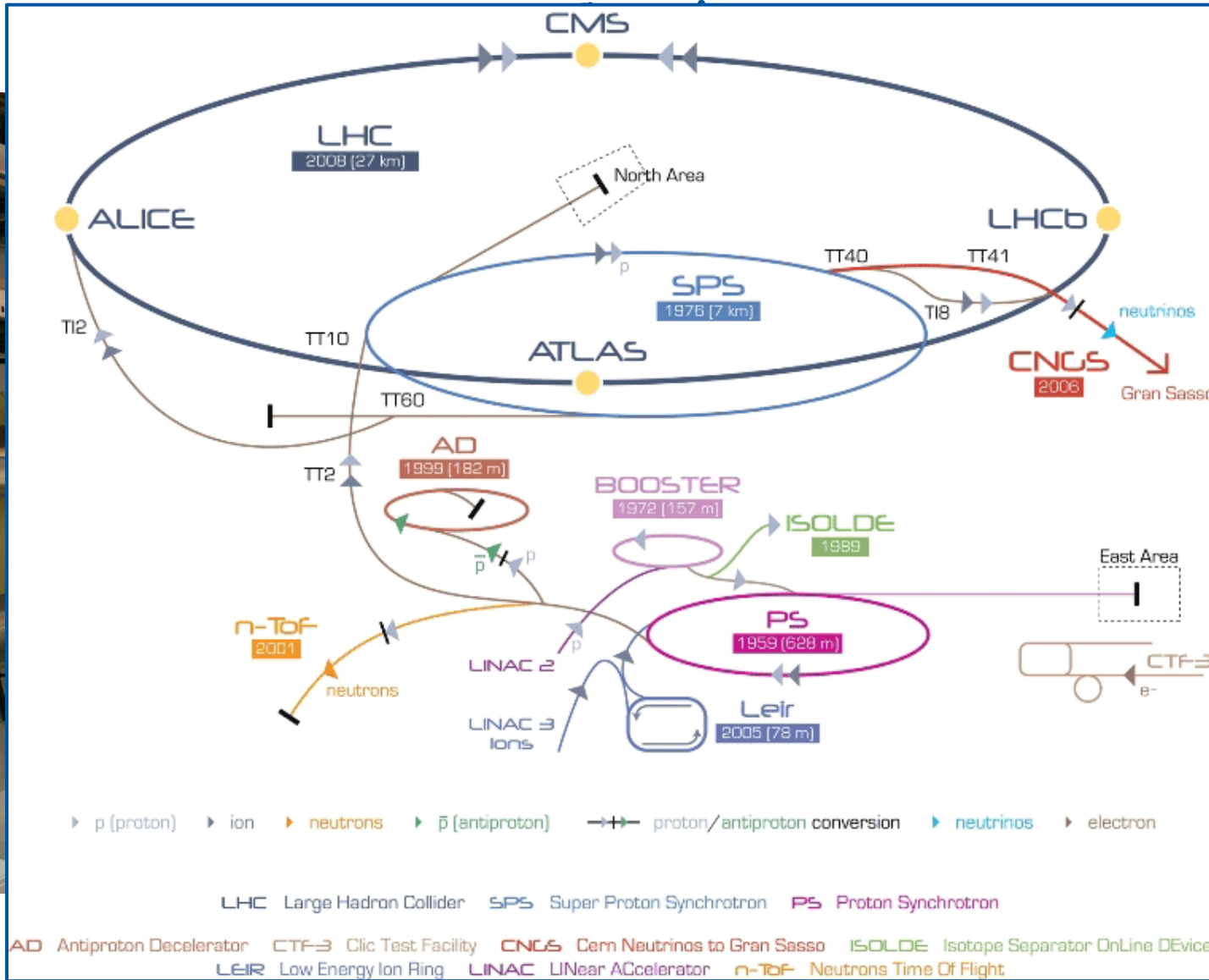
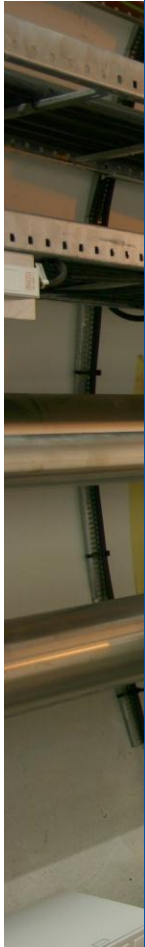
Part 1

Introduction

- a) The vacuum system design philosophy depends on the type of accelerator: circular storage rings and linear accelerators have in general different vacuum requirements and therefore very different chamber geometries
- b) A storage ring has to keep the beam(s) stored for up to tens of hours, while linear colliders have much shorter beam transit and vacuum feed-back times (although the repetition rate plays a role)
- c) The geometry of the chamber is generally much dependent on other accelerator components' design and requirements: in particular, the vacuum chamber cross-section is a balance between **i)** the beam size envelope (with related sigmas, orbit excursions, and alignment tolerances) and **ii)** the inscribed circle of the quadrupoles (and/or gap opening of the dipoles). Designing the largest possible cross-section (i.e. conductance) by maximizing i) and minimizing ii) is one of the most important steps leading to a successful vacuum system design
- d) A clear difference in chamber geometry stems also from the magnet technology, i.e. superconducting (SC) technology vs room-temperature (RT) one. By its very nature SC magnets call for circular geometries (e.g. LHC) while RT magnets leave more freedom to the design of the vacuum chamber (e.g. synchrotron radiation (SR) light sources)

- e) The material chosen for the fabrication of the vacuum chamber also plays an important role in the design, as it dictates the thickness of the vacuum chamber, and its capability to be baked (and therefore the attendant outgassing rate and ultimate gas composition)
- f) The beam lifetime requirements dictate the highest average pressure tolerated by the beam or the experiments (background, radiation damage, etc...). This parameter, coupled with the previous ones determines the minimum effective pumping speed which has to be attained at the end of the machine commissioning phase. The equation $S_{\text{eff}} = (1/S_{\text{inst}} + 1/C)^{-1}$ tells the designer what pumping speed will need to be installed, and this relation makes it clear the importance of maximizing the (specific) conductance of the vacuum chamber, in order to reduce capital costs
- g) Vacuum-wise, there are two types of vacuum chambers: “cylindrical” ones, where the cross-section stays +/- the same over its length (e.g. LHC arcs, transfer lines), and “variable cross-section” ones, where the cross-section changes frequently (e.g. SR light sources)

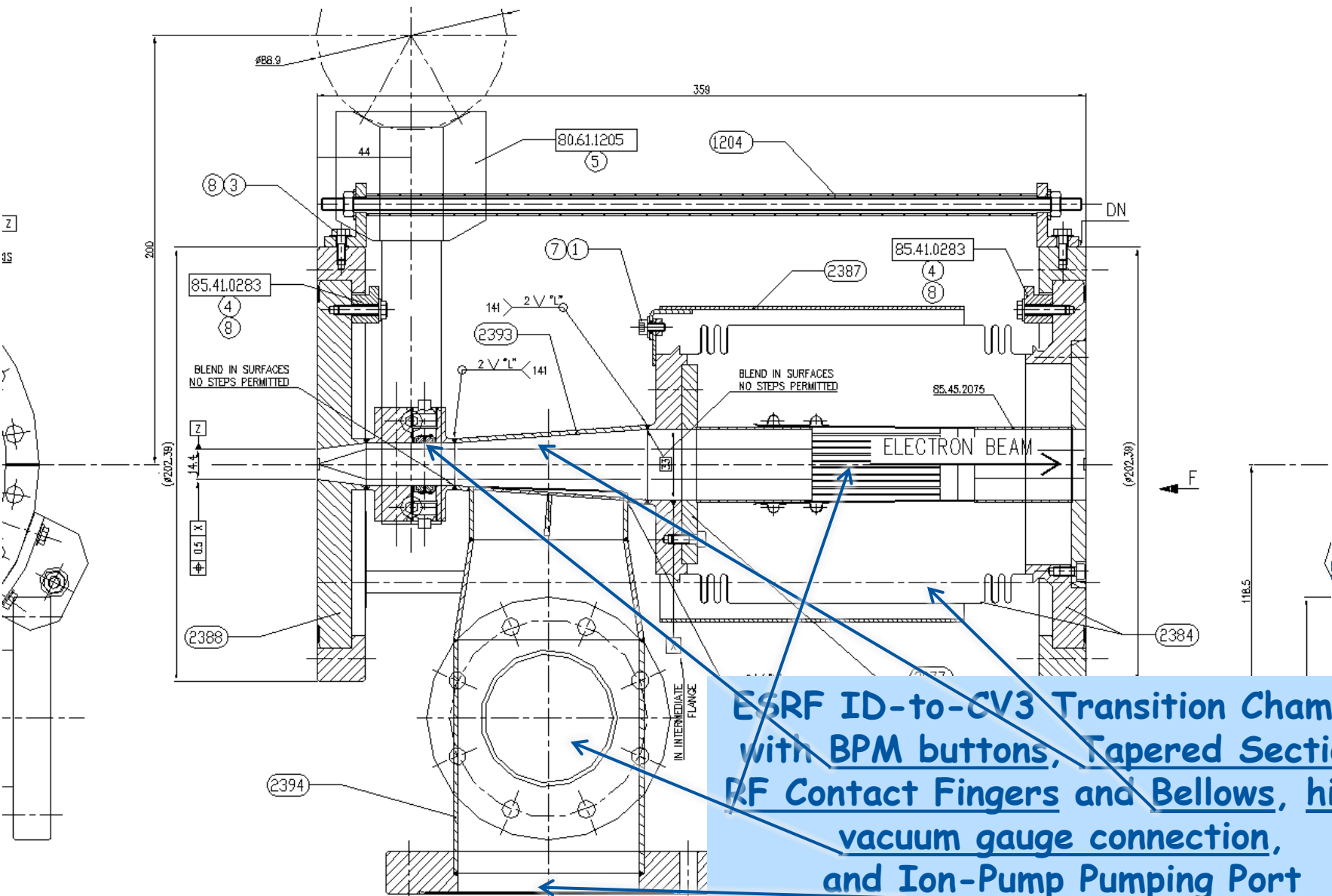
An SPS-to-LHC Transfer Line in the Accelerator



ion pump)
T"

Courtesy:





ESRF ID-to-CV3 Transition Chamber with BPM buttons, Tapered Section, RF Contact Fingers and Bellows, high-vacuum gauge connection, and Ion-Pump Pumping Port

j) Different types of accelerators are affected by different types of outgassing profiles:

1. Static thermal outgassing (e.g. unbaked transfer lines)
2. SR-induced outgassing (e.g. light sources, e^+e^- B-factories, LHC at energies $>2.0\sim 2.5$ TeV)
3. Ion-induced outgassing (e.g. LHC)
4. Electron cloud-induced desorption (e.g. SPS, LHC)
5. Cryogenic "recycling" (e.g. LHC)
6. Combination of all or some of the above (e.g. LHC, which can be affected by all of them)

This presentation will focus mainly on the analysis and conceptual design of the geometry of the vacuum chamber vs the type of accelerator, and its effects on the pressure profiles

Part 2

Analytical and Numerical Methods

- a) At the onset of accelerator technology, several analytical formulae have been obtained by physicists and engineers working on vacuum systems, for the calculation of:
 1. Conductances
 2. Pumping speeds
 3. Outgassing rates
 4. Pressure profiles

- b) As the accelerators have evolved and diversified during the following decades, the limits of the analytical methods have become clear, and several numerical algorithms have been devised:
 1. Continuity Principle of Gas Flow (CPoGF)
 2. Finite-Elements
 3. Applications of Diffusion Equations
 4. Montecarlo Simulations (MC)

- c) In particular, the exponential improvement in computing power and the dramatic decrease of hardware costs have put the MC method in front of the others, allowing a direct transfer of CAD geometries to the MC simulation software, thus streamlining design & integration issues

The Flow of Highly Rarefied Gases through Tubes of Arbitrary Length

P. Clausing

Natuurkundig Laboratorium, N. V. Philips' Gloeilampenfabrieken, Eindhoven, The Netherlands
(Received 26 November 1931)

Editor's Note: Translated from the German [*Ann. Physik* (5) 12, 961 (1932)]. Since this classic paper is referred to so frequently by workers in vacuum technology, it has been decided to publish an English translation. The translation was made available through the courtesy of Veeco Instruments, Inc., who also supported its publication.

Contents

(I) The expressions of Knudsen, v. Smoluchowski, and Dushman for steady-state molecular flow; (II) transformation of the equations to kinetic variables, transmission probability; (III) derivation of the Dushman formula; (IV) the problem of the short, round cylindrical tube; (V) the problem of the long, round cylindrical tube; (VI) the application of the flow equation in high-vacuum engineering; summary.

I. The Expressions of Knudsen, v. Smoluchowski, and Dushman for Steady-State Molecular Flow

Knudsen¹ has given the following expression for the steady flow of a highly rarefied gas through a tube of arbitrary cross section

$$J = \frac{8}{3} \frac{2\sqrt{\pi}}{\pi} \frac{S^2}{L} \frac{1}{(d)^3} (\rho_1 - \rho_2), \quad (1)$$

where J is the amount of gas flow per second, measured by the volume it would occupy at unit pressure, d is the density of the gas at unit pressure, S is the cross-sectional area of tube, s is the circumference of the cross section, and L is the length of the tube. ρ_1 and ρ_2 are the pressures in the two volumes connected by the tube, and we assume that the first is always to the left of the second (the indices 1 and 2 in this article refer exclusively to the two volumes).

For the derivation it is assumed that L is very large in comparison both to the transverse dimensions of the cross section of the tube as well as to the mean free path of the molecules, and further, that the molecules leave the wall of the tube diffusely in accordance with the cosine law.²

For a long circular cylindrical tube with radius r ,

Eq. (1) gives

$$J = \frac{4(2\pi)^{3/2} r^3}{3 L (d)^3} (\rho_1 - \rho_2). \quad (2)$$

For an orifice in a very thin wall, Knudsen² found

$$J = S / (2\pi)^{1/2} \cdot 1/d^3 (\rho_1 - \rho_2), \quad (3)$$

which gives for a circular opening

$$J = (\pi/2)^{1/2} \cdot r^3/d^3 (\rho_1 - \rho_2). \quad (4)$$

M. v. Smoluchowski³ has shown that Eq. (1) is not correct and that it should be replaced with

$$J = \frac{1}{2} \frac{A}{(2\pi)^{1/2}} \frac{1}{L} \frac{1}{(d)^3} (\rho_1 - \rho_2),$$

where

$$A = \int_0^{\pi/2} \int_{-\pi/2}^{\pi/2} \frac{1}{2} \rho^2 \cos \theta d\theta ds, \quad (5)$$

in which ρ represents a chord of the cross section, which forms an angle θ with the normal to ds .⁴ It is probably accidental that Eq. (2) is correct; for the circular cylinder the error of the Knudsen equation is removed.

As stated, Eqs. (2) and (5) apply only for relatively long tubes. When $L=0$ the result would be that $J = \infty$ in both cases instead of changing to Eq. (3).

Dushman^{5,6} was the first to propose an expression which applies also to short tubes and which, for $L=0$, does not give $J = \infty$, but rather Eq. (3). (For practical reasons Dushman considered only circular cylindrical tubes and round orifices.)

A second expression has been derived by the author.^{7,8,9} Although it gives the same results as the Dushman formula for $L/r=0$ and $L/r = \infty$ [Knudsen's Eqs. (2) and (4)], the two equations deviate considerably from each other in the intermediate region. In

a.1) Conductances

- P. Clausing (1931)
- W Steckelmacher (1966)

Vacuum/volume 16/number 11. Pergamon Press Ltd/Printed in Great Britain

A review of the molecular flow conductance for systems of tubes and components and the measurement of pumping speed

W Steckelmacher, Edwards High Vacuum International Ltd, Manor Royal, Crawley, Sussex

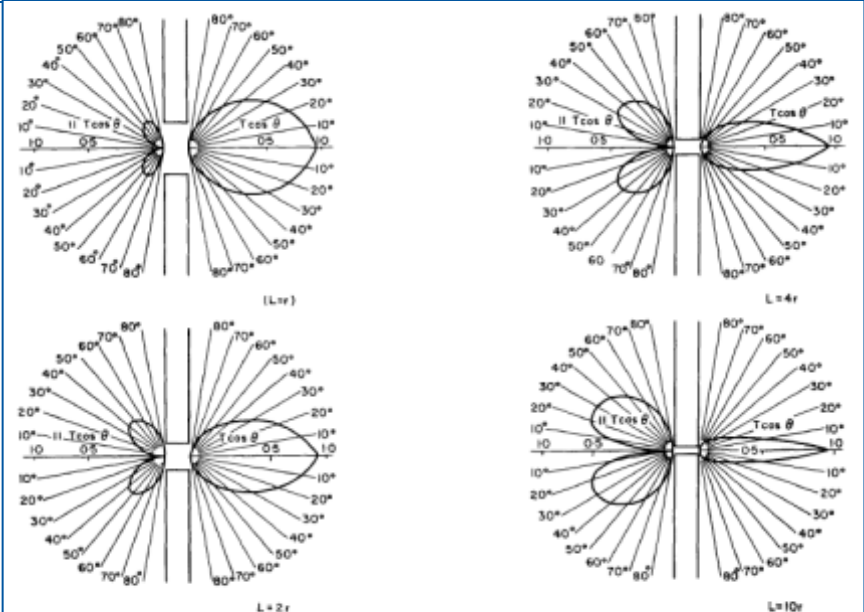
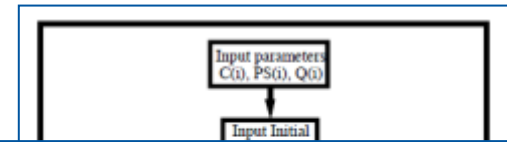


Figure 4. Polar diagrams of gas flow at entrance and exit of cylindrical tubes when $L/r=1$, $L/r=2$, $L/r=4$ and $L/r=10$, (calculated by Dayton, 1957).

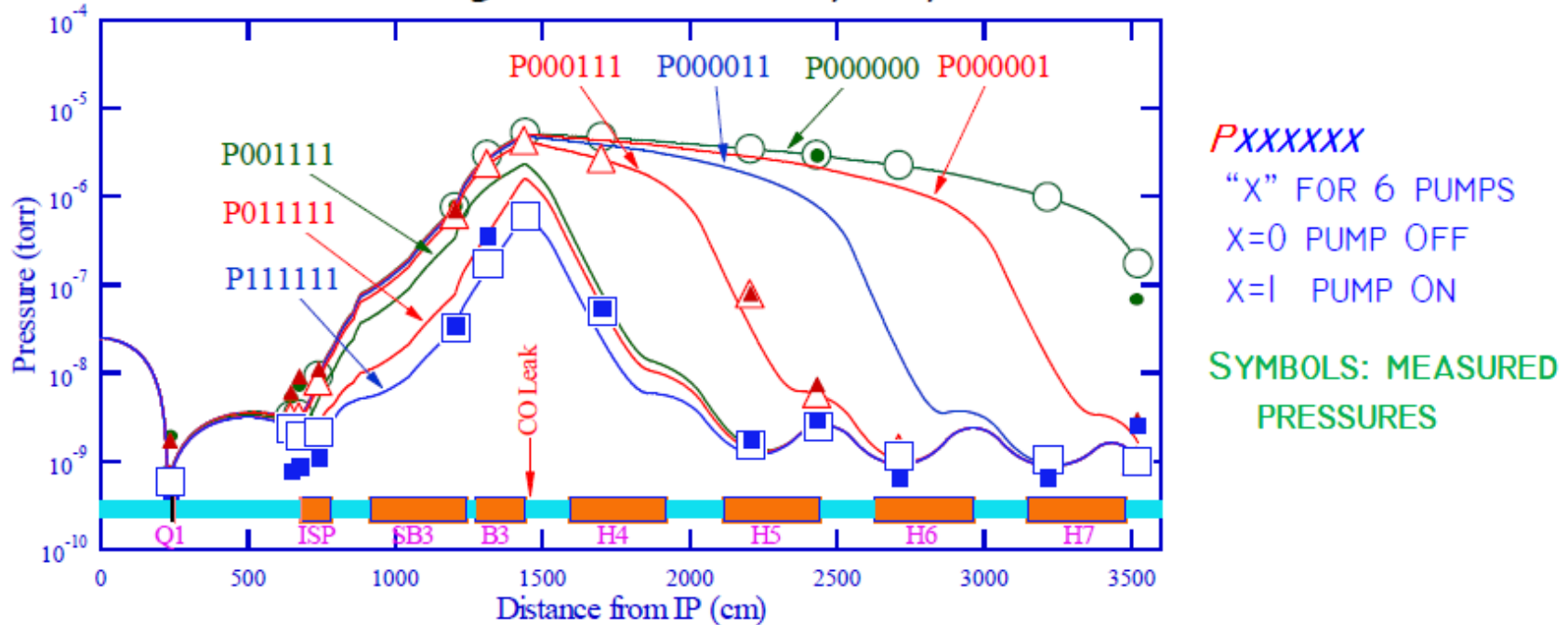
"beaming effect"

b.1) Pressure profile

- Y. Li (1995): example of FEM for calculating pressure profiles in the CESR accelerator



In CESR/CLEO HEP II operations, an experiment was conducted to probe the HEP detector background sensitivity to pressure distribution



- *In the experiment, a CO gas was introduced to create a 'pressure bump', and ion pumps (2 LPs, 4 DIPs) were turned off sequentially to spread the bump. A probe electron beam was sent through the bump to measure detector background.*
- *Pressure profiles were calculated and compared to the measured pressures, with ion pump speed's pressure dependence taking into account.*
- *The results helped design of background masks for the CESR/CLEO III upgrade.*

Courtesy of Y. Li, LAPP, Cornell University, see ref., session 5.1

a.2) Pumping speeds
 R. Kersevan et al.
 (1997)

MASSIVE TITANIUM SUBLIMATION PUMPING IN THE CESR INTERACTION REGION[†]
 N.B. Mistry, R. Kersevan and Yulin Li,
 Laboratory of Nuclear Studies, Cornell University, Ithaca, NY 14853 USA

**CESR: e^+e^- collider,
 5.3 GeV/beam
 B-meson studies and
 'parasitic' SR light
 source**

*Abstract**
 The residual gas pressure within 30 m of the interaction point (IP) at the e^\pm collider CESR is maintained in the low nanotorr range despite the high gas loads produced by the intense flux of synchrotron radiation from the electron and positron beams. A low pressure is necessary in order to minimize the experimental backgrounds due to beam gas scattering. Within 12 m of the IP, the vacuum chambers incorporate large pumping plenums with massive titanium sublimation pumping to provide the necessary pumping speed and capacity. Operating experience over the last two years has shown that this method of pumping is efficient and inexpensive.

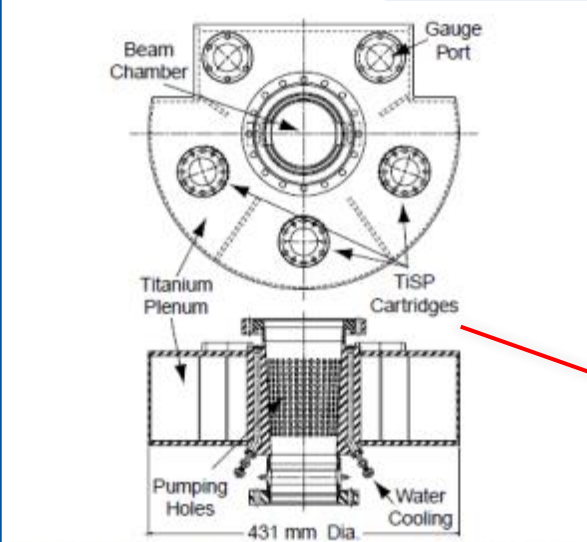


Figure 1. The Q1 titanium pump chamber. Above, view along beam. Below, cross-section looking down.

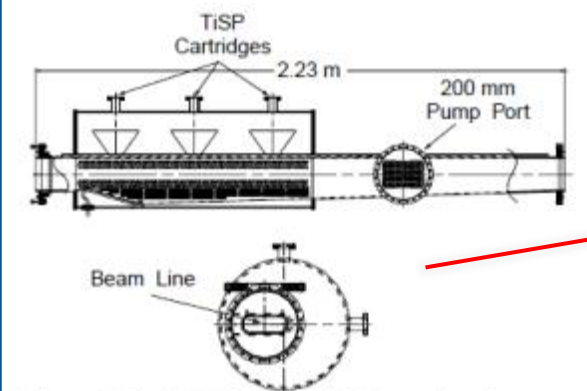


Figure 2. The ISP Chamber with Ti pumping plenum.

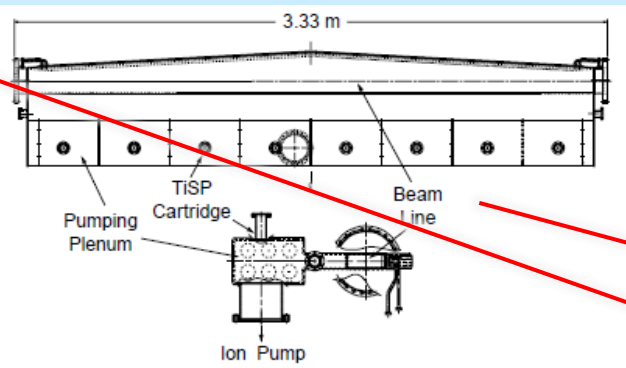


Figure 3. The Soft-Bend Chamber. Top view (above) and cross-section showing Ti pumping plenum.

TABLE I. Synchrotron Radiation Flux and Gas Load in the CESR IR for 300 mA e^\pm Stored Beams.

Location	Flux Density (Photon/s/m)	Total Flux (Photons/s)	CO GasLoad [Torr-l/s]
Q1-Pump	$1.3 \cdot 10^{18}$	$2.5 \cdot 10^{17}$	$7.9 \cdot 10^{-8}$
ISP absorb.	$1.1 \cdot 10^{19}$	$1.9 \cdot 10^{18}$	$2.0 \cdot 10^{-7}$
Soft-Bend	$3.3 \cdot 10^{18}$	$3.5 \cdot 10^{18}$	$6.7 \cdot 10^{-7}$
Hard-Bend	$6.9 \cdot 10^{18}$	$2.3 \cdot 10^{19}$	$1.3 \cdot 10^{-6}$

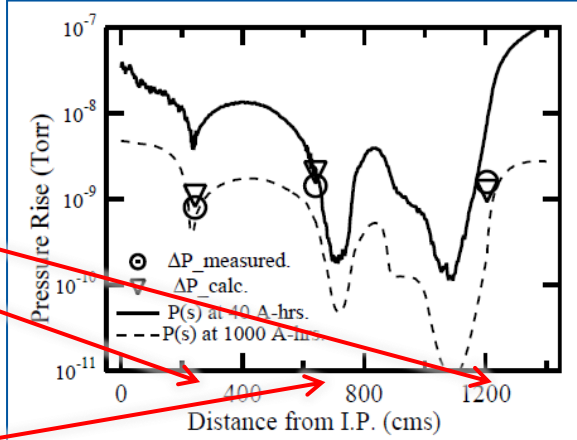


Figure 8: The calculated profile of the beam induced pressure rise on the beam line, $\Delta P(s)$, and the measured values obtained during an HEP run with 94 mA e^- and 122 mA e^+ in CESR. Note that the ΔP measured and calculated for gauges at Q1 (at 540 cm) & SoftBend (at 1200 cm) are much lower than the curve as the CCGs are not installed directly on the beam chamber, but rather on the pumping plenums. The solid curve refers to an early stage of conditioning, after a beam dose of 40 Amp-hrs. The dotted pressure profile is for 150 mA e^\pm beams after 1000 A-hrs of running.

Introduction to MOLFLOW+: New graphical processing unit-based Monte Carlo code for simulating molecular flows and for calculating angular coefficients in the compute unified device architecture environment

R. Kersevan^{a)} and J.-L. Pons
 European Synchrotron Radiation Facility, 38043 Grenoble, France

(Received 14 November 2008; accepted 18 May 2009; published 30 June 2009)

The authors present here the description of the main features of MOLFLOW+, a new software package that allows the calculation of several physical quantities of interest to vacuum engineers and scientists, such as pressure profiles, effective pumping speeds, adsorption distributions, angle of incidence or effusion profiles, and more. MOLFLOW+ is a follow up to the code MOLFLOW, which has been developed by one of us since 1991, and used for the analysis and design of many vacuum systems and components. MOLFLOW+ makes use of modern trends such as OpenGL graphic interface, multicore processors, graphical processing units (GPUs), and runs under different operating systems. In addition to implementing the test-particle Monte Carlo (TPMC) algorithm, as done previously in MOLFLOW, MOLFLOW+ also implements an alternate algorithm, the angular coefficient (AC) method. This article goes into some details of the TPMC and AC methods as implemented in MOLFLOW+, shows results of benchmark runs and comparisons with published numerical and analytical data, and discusses the advantages and disadvantages of the two methods. CUDA is the compute unified device architecture, a C++-like development environment for a class of GPUs. © 2009 American Vacuum Society. [DOI: 10.1116/1.3153280]

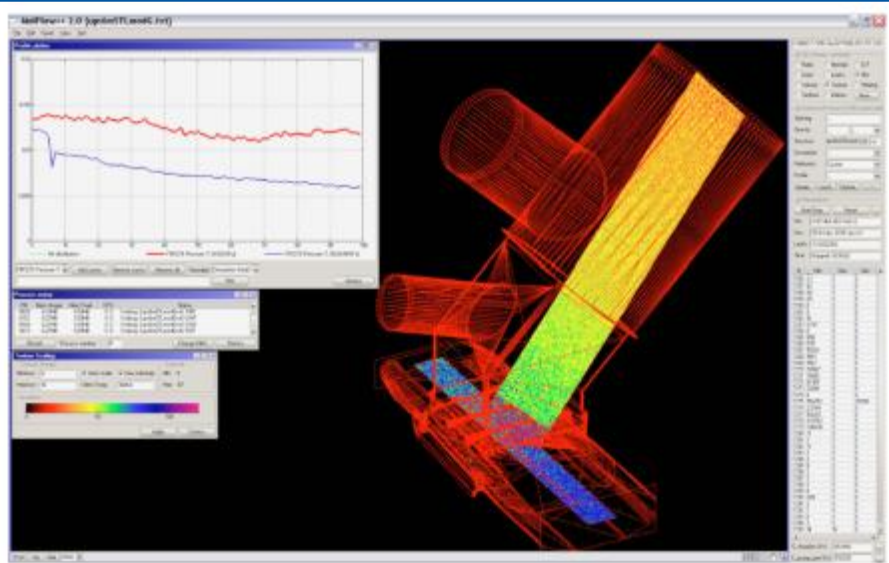
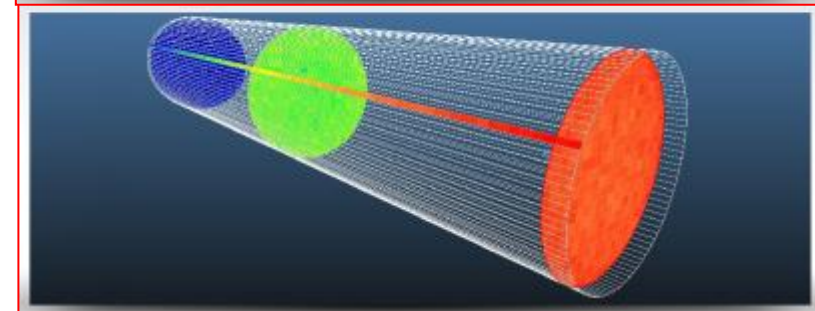
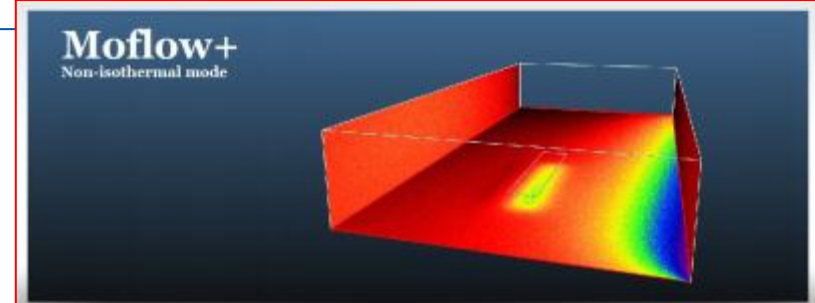


FIG. 10. (Color online) Screen capture of the TPMC calculation of the pressure profiles and effective pumping speed for a 45° pumping port. Upper curve (red line on paper online): pressure along the e-beam chamber; lower curve (blue line): pressure along 45° tube (from beam line up toward the pump). A 150 l/s ion pump is assumed to be installed. Effective pumping speed along the e-beam path, derived from the average of the red curve, is 80.3 l/s. Total time taken by quad-core, 2.33 MHz CPU was 18 min, ~25 000 molecules desorbed. Original STP/STL files courtesy of Coulon, Mechanical Engineering Group, ESRF.

b.4) Test-Particle Montecarlo (TPMC) simulations

- R. Kersevan et al. (2008);
- R. Kersevan, M. Ady (2012);



Status of the FRIB Driver Linac Vacuum Calculations

Bojan Đuričković*† Paul Gibson* Roberto Kersevan‡

DRAFT, version 0.9
January 15, 2013

Abstract

The Facility for Rare Isotope Beams (FRIB) is a superconducting heavy ion linear accelerator that is to produce rare isotopes far from stability for low energy nuclear science. In order to achieve this, its driver linac needs to achieve a very high beam current (up to 400 kW beam power), and this requirement makes vacuum levels of critical importance. Vacuum calculations have been carried out to verify that the vacuum system design meets the requirements. In this paper, we present an overview of the methods used for FRIB vacuum calculations and simulation results for some interesting sections of the accelerator.

b.4) Test-Particle Montecarlo (TPMC) simulations

- B.Durickovic, R. Kersevan, P.Gibson, submitted to JVST A

Location in driver linac	Average Pressure [Torr]	Comment
FE Ion Source Injection Region	$< 3 \times 10^{-7}$	
FE Ion Source Extraction Region	$< 1 \times 10^{-7}$	
FE Charge Selection System	$< 3 \times 10^{-8}$	
FE LEBT	$< 5 \times 10^{-9}$	
FE RFQ	$< 5 \times 10^{-8}$	
FE MEBT	$< 1 \times 10^{-8}$	
LS1	$< 5 \times 10^{-9}$	In the warm regions
FS1 Charge Stripping section	$< 1 \times 10^{-8}$	Near the matching CMs
FS1 Charge Stripping section	$< 1 \times 10^{-6}$	Near the Li stripper
FS1 Beam Bending Section	$< 5 \times 10^{-8}$	After the second 45° dipole
FS1 Matching Section	$< 5 \times 10^{-9}$	
LS2	$< 5 \times 10^{-9}$	In the warm regions
FS2	$< 1 \times 10^{-8}$	
LS3	$< 5 \times 10^{-9}$	In the warm regions
LS3 Beam Transport Section	$< 1 \times 10^{-8}$	
BDS	$< 1 \times 10^{-8}$	

Table 1: FRIB driver linac vacuum requirements: beam line vacuum pressure during operation [1]. The Charge Stripping section requirements are based on lithium charge stripping. (FE=Front End, LS=Linac Segment, FS=Folding Segment, BDS=Beam Delivery Segment)

3.6 Transmission rate calculations

In the Front End, we considered transmission rates in conjunction with required pressure levels. The main source of beam loss is charge exchange (electron pickup from residual gas) $X^q + R \rightarrow X^{q-1} + R^+$, where X^q is the accelerated beam ion (in charge state q), and R designates the residual gas. The beam transmission is given by

$$T = \exp\left(-\int_0^L n \sigma_{q,q-1} dz\right), \quad (1)$$

where z is the length coordinate along the beam axis, L is the beam line length, $n = n(z)$ is the residual gas concentration, $\sigma_{q,q-1}$ is the charge exchange cross section given by Salzbren and Müller [2]:

$$\sigma_{q,q-1} = 1.43 \times 10^{-12} q^{1.17} \left(\frac{I}{IV}\right)^{-2.76} \text{ cm}^2, \quad (2)$$

and I is the first ionization potential of the residual gas. The charge pickup cross section decreases with energy if energy is higher than a few tens keV, but the beam energy up to the radio frequency quadrupole (RFQ) is low enough that this formula applies.

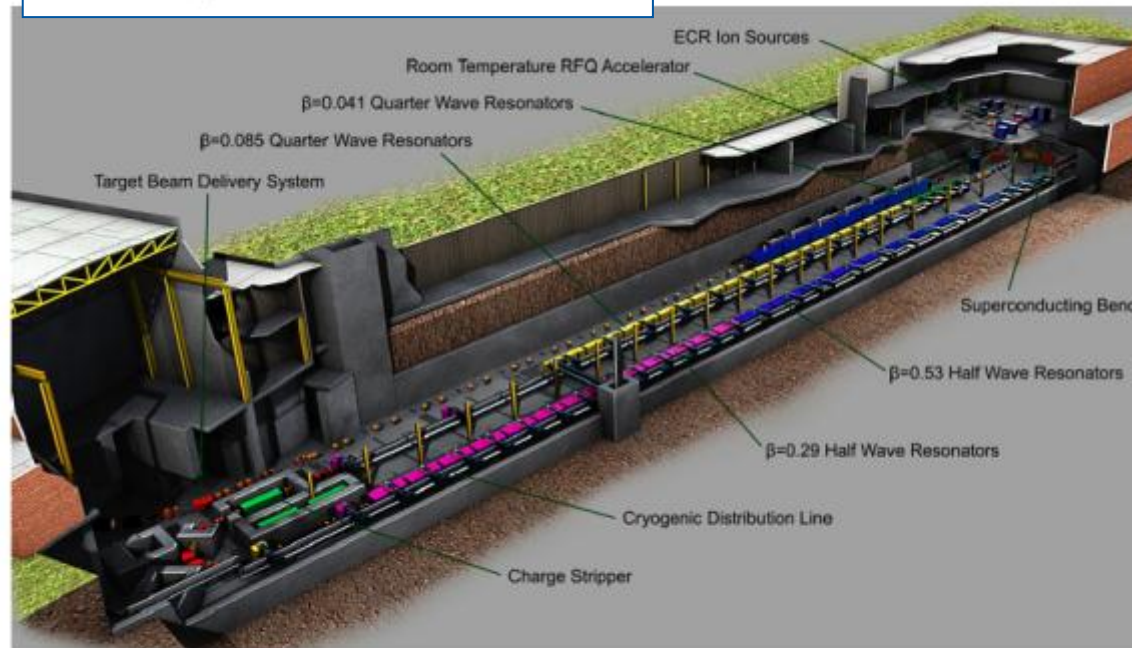
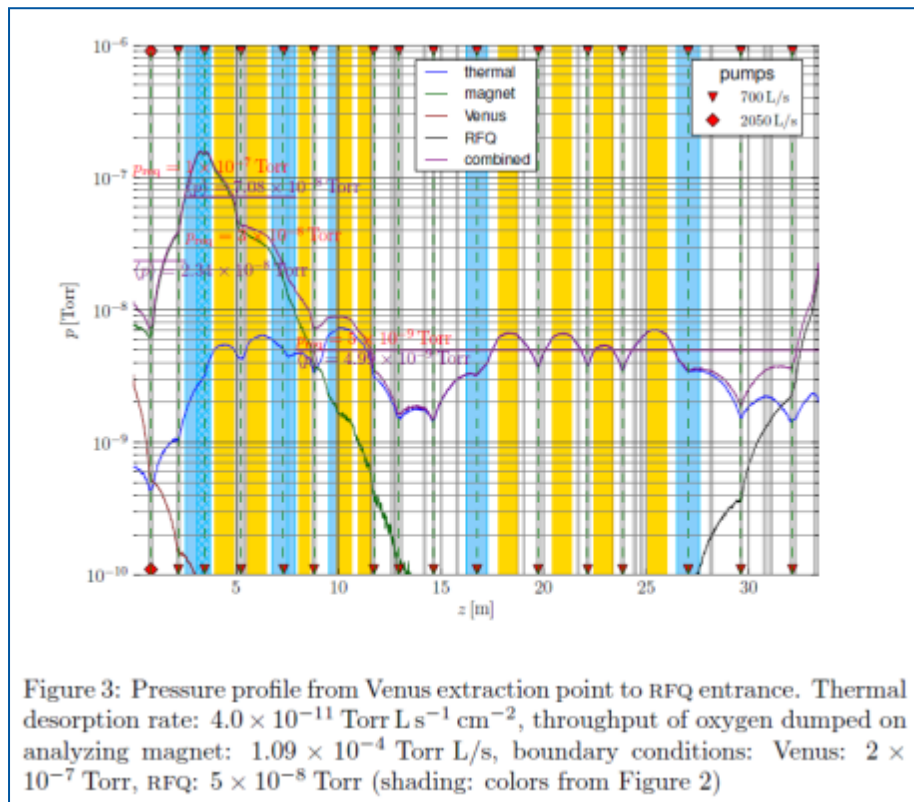
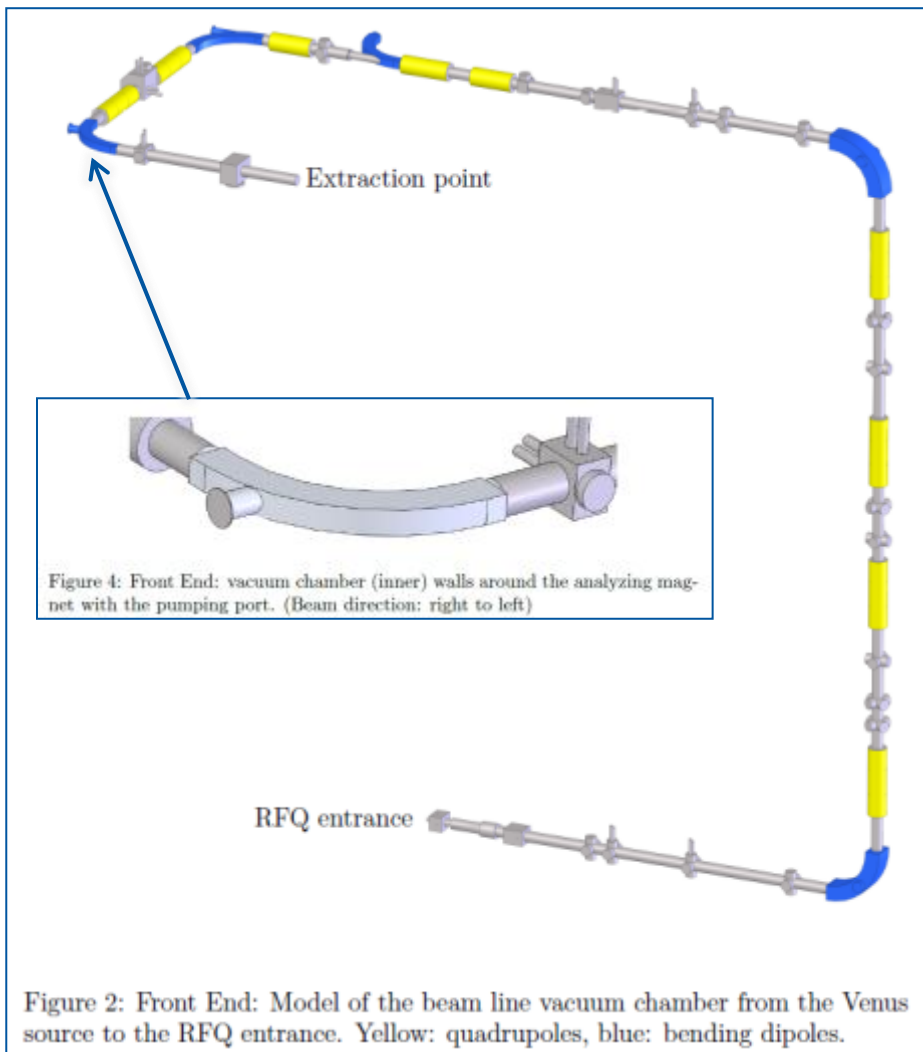


Figure 1: FRIB driver linac

Aim: minimize charge-exchange ionization losses

b.4) Test-Particle Montecarlo (TPMC) simulations (Molflow+)

- B.Durickovic, R. Kersevan, P.Gibson, submitted to JVST A



Part 3

Vacuum Chamber Geometries By Examples

- a) As mentioned before, different accelerators come with different vacuum chamber geometries
- b) Most often it is the cross-section's size which is different. Some extreme examples are:
 1. The Spallation Neutron Source (SNS) accumulation ring has a round circular cross-section of large internal diameter (ID~300 mm)
 2. One of the proposed geometries for the CLIC quadrupoles linac has a "butterfly" cross-section (so called "antechamber"), with a central circular pipe of less than 10 mm ID
 3. The LHCb experimental chamber has a conical shape with ID going from 50 to 260 mm
 4. The insertion device (ID) vacuum chambers of the ESRF light source have an elliptical cross-section of 57x8 mm² (HxV) axis
 5. LHC SC dipole arc sections: 1.9K cold bore with inserted 5-20K beam screen with pumping slots. Material is stainless steel, with co-laminated copper coating on the inside and sawtooth SR absorber

1. The Spallation Neutron Source (SNS) accumulator ring has a round circular cross-section of large internal diameter (ID~ 260 mm)

Proceedings of the 1999 Particle Accelerator Conference, New York, 1999
DESIGN OF THE SNS ACCUMULATOR RING VACUUM SYSTEMS*
 H.C. Hseuh[†], C.J. Liaw, M. Mapes, BNL, Upton, NY 11973

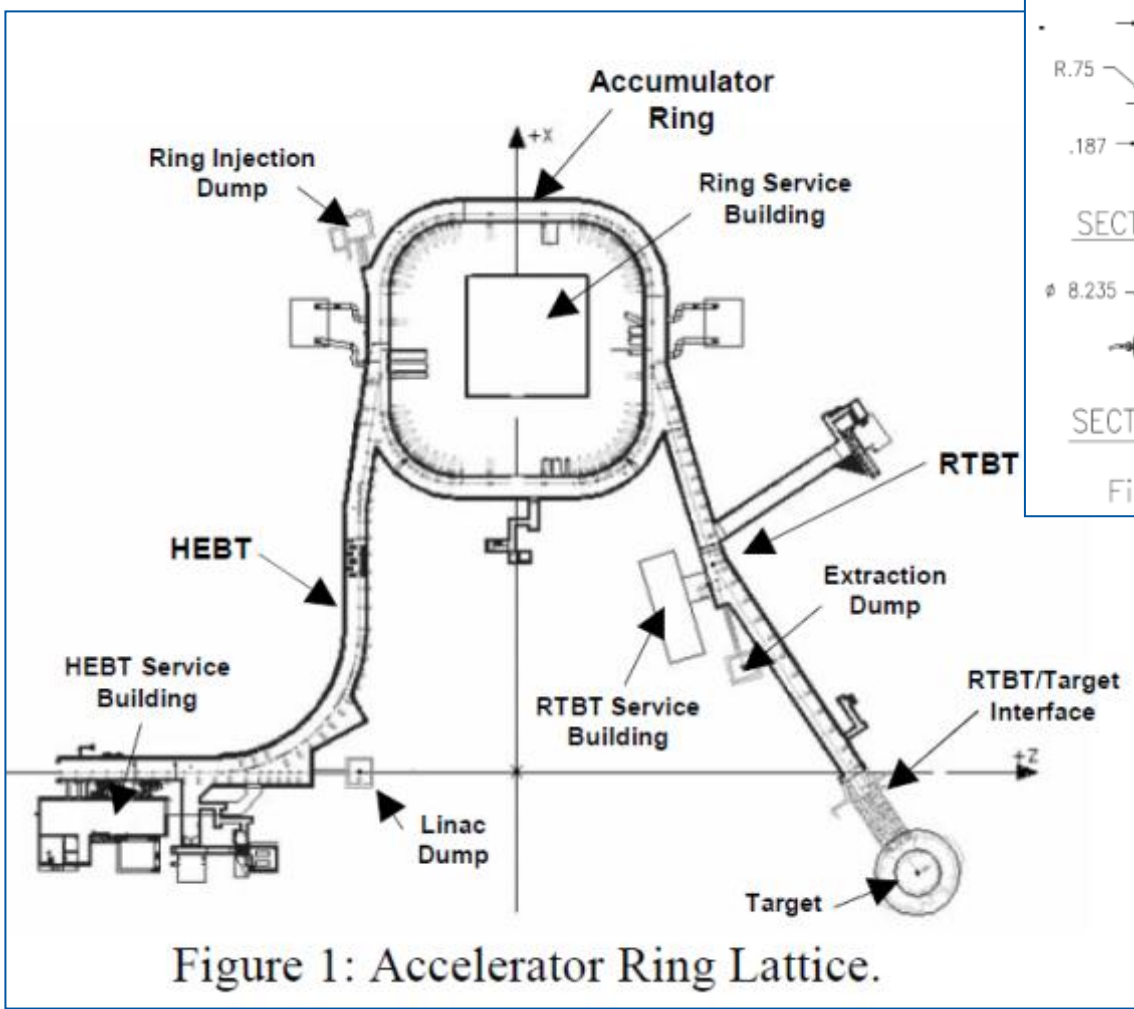


Figure 1: Accelerator Ring Lattice.

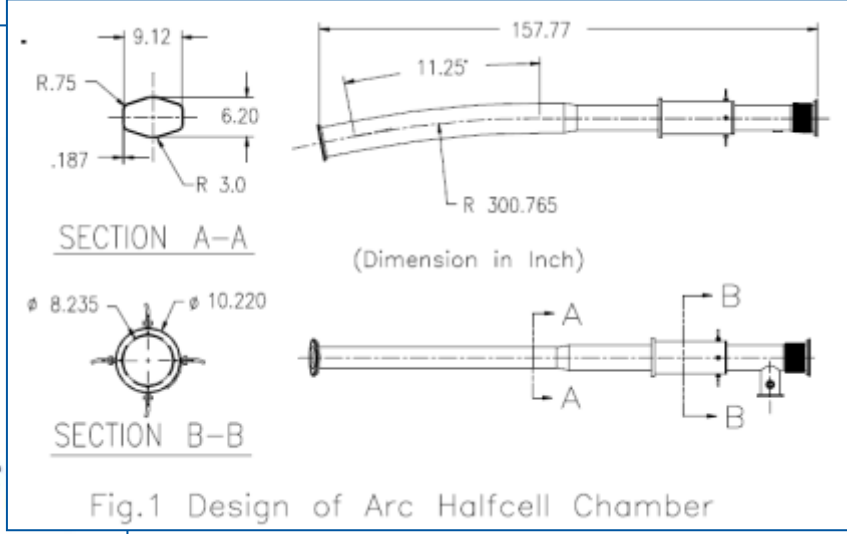


Fig.1 Design of Arc Halfcell Chamber

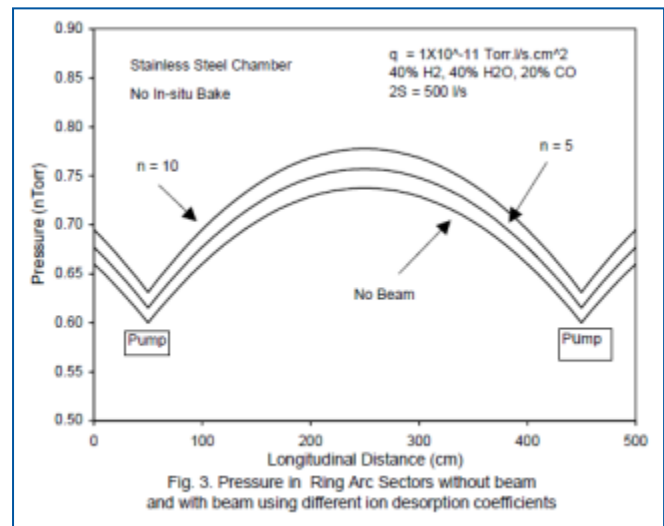


Fig. 3. Pressure in Ring Arc Sectors without beam and with beam using different ion desorption coefficients

2. One of the proposed geometries for the CLIC quadrupoles linac has a “butterfly” cross-section, with a central circular pipe of 10 mm OD

Proceedings of PAC09, Vancouver, BC, Canada

MO6RFP007

DESIGN OF THE CLIC QUADRUPOLE VACUUM CHAMBERS

C. Garion, H. Kos, CERN, Geneva, Switzerland

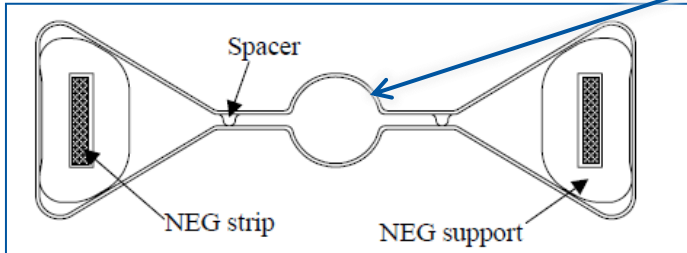


Figure 1: Concept of the vacuum chamber

The effective pumping speed per unit length of the central part is defined as:

$$\frac{1}{S_{eff}} = \frac{1}{S} + \frac{1}{C_g}$$

with S the pumping speed of unit length of NEG strip. C_g stands for the unit conductance of the gap between the central part and the antechamber. It is obtained from the conductance of a rectangular duct:

$$Cr = \frac{2}{3} \frac{h^2 w^2}{(h+w)L} \bar{v}$$

with L the length of the duct. h and w denote the height and the width of the duct, respectively. \bar{v} is the average molecular velocity. In our case, $h \ll w$ thus the unit conductance of the gap C_g can be written as:

$$C_g = \frac{2}{3} \frac{h^2}{L} \bar{v}$$

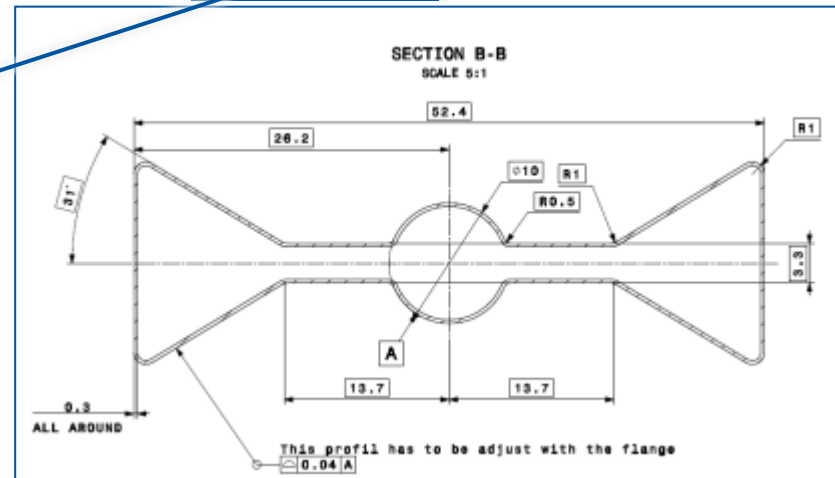
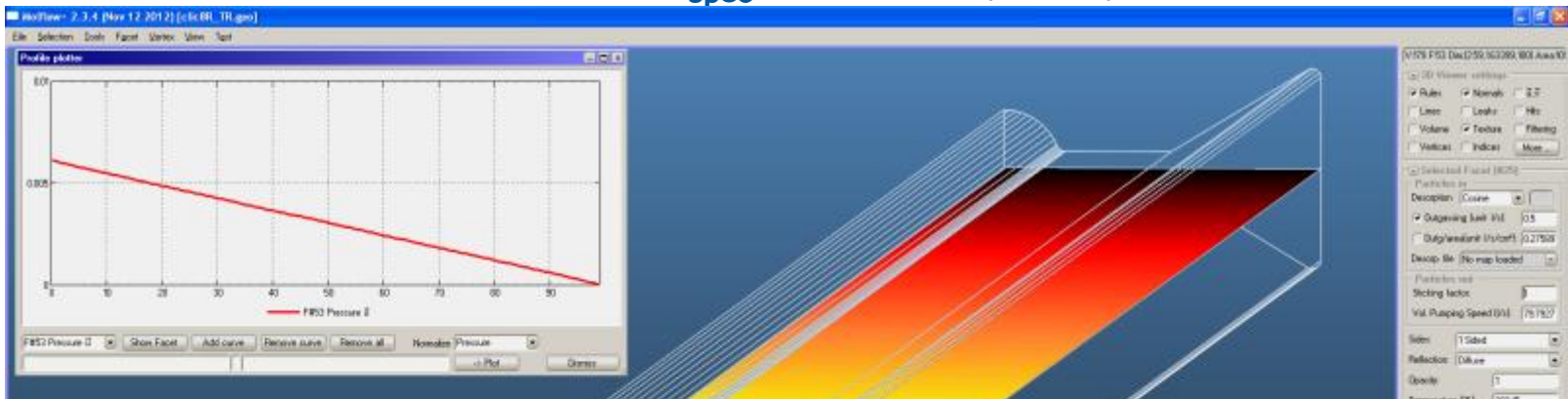


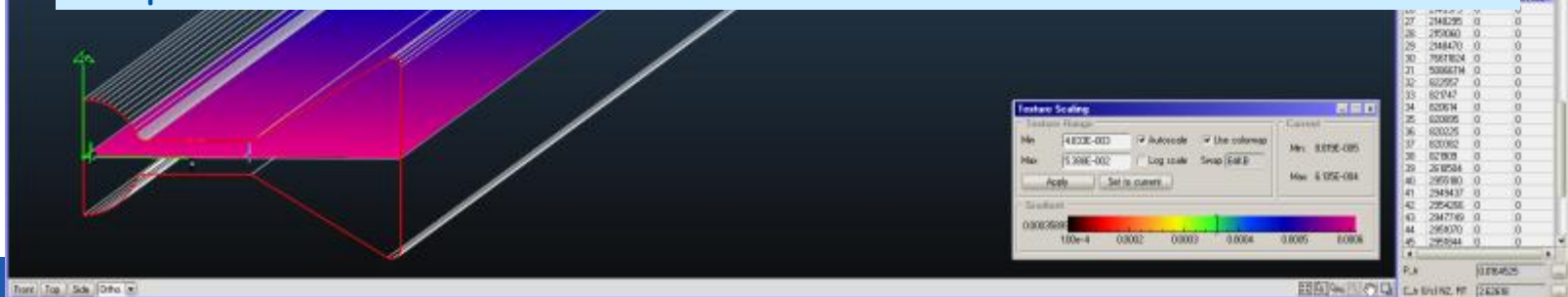
Figure 4: Test set-up of the vacuum chamber

2. TPMC/Molflow+ calculation of the specific conductance of the CLIC quadrupole cross-section (method 1): one plane of symmetry (w/ mirror reflection), $\frac{1}{2}$ of the chamber is modeled; Molecules are generated on entrance (on the left), pumped at entrance and exit (sticking=1); ratio of exiting to generated molecules is the transmission probability P_{TR} , $P_{TR}=0.01645$; Specific conductance is obtained by multiplying P_{TR} by entrance area (cm^2) by 11.77 (l/s/cm^2) (N_2 gas at 20 C): $C_{\text{spec}} = 2.626$ ($\text{l}\cdot\text{m/s}$)

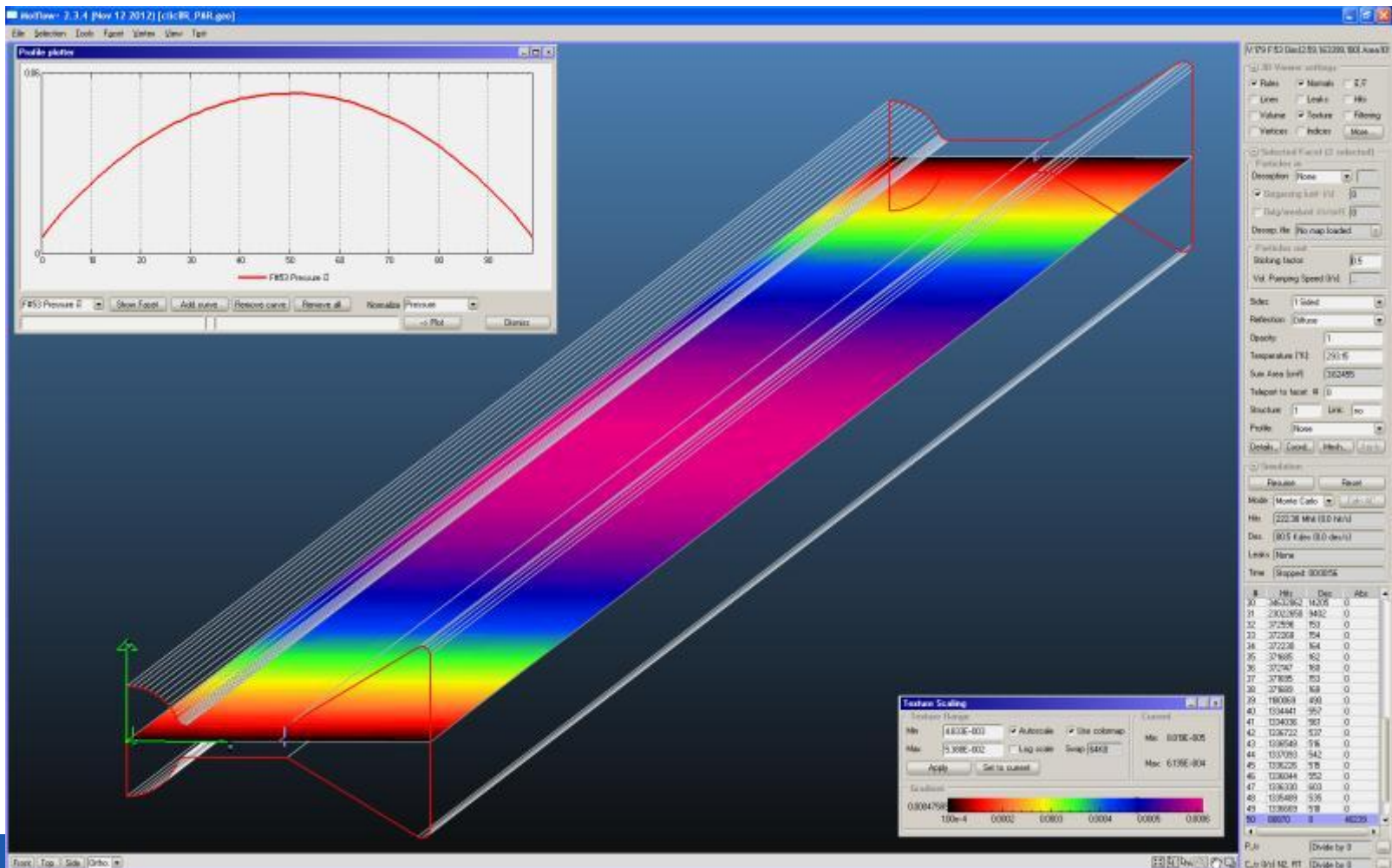


By comparison, the transmission probability of the round tube only would be, $P_{TR}=0.0122$; Specific conductance obtained by multiplying P_{TR} by entrance area (0.694 cm^2) and by 11.77 (l/s/cm^2) (N_2 gas at 20 C):

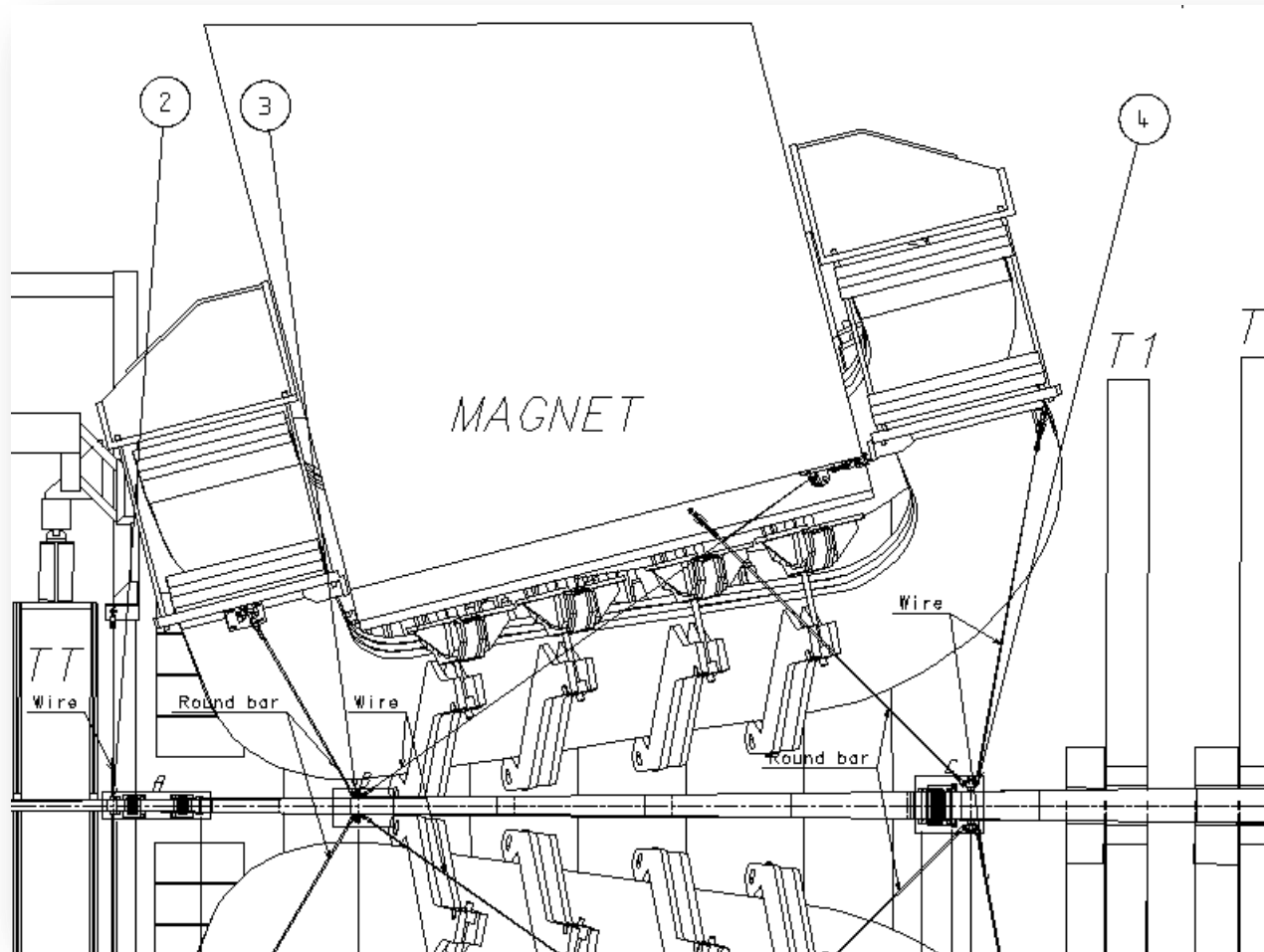
$$C_{\text{spec}} = 0.0994 \text{ (l}\cdot\text{m/s) (only 3.8\% of the "butterfly" profile)}$$



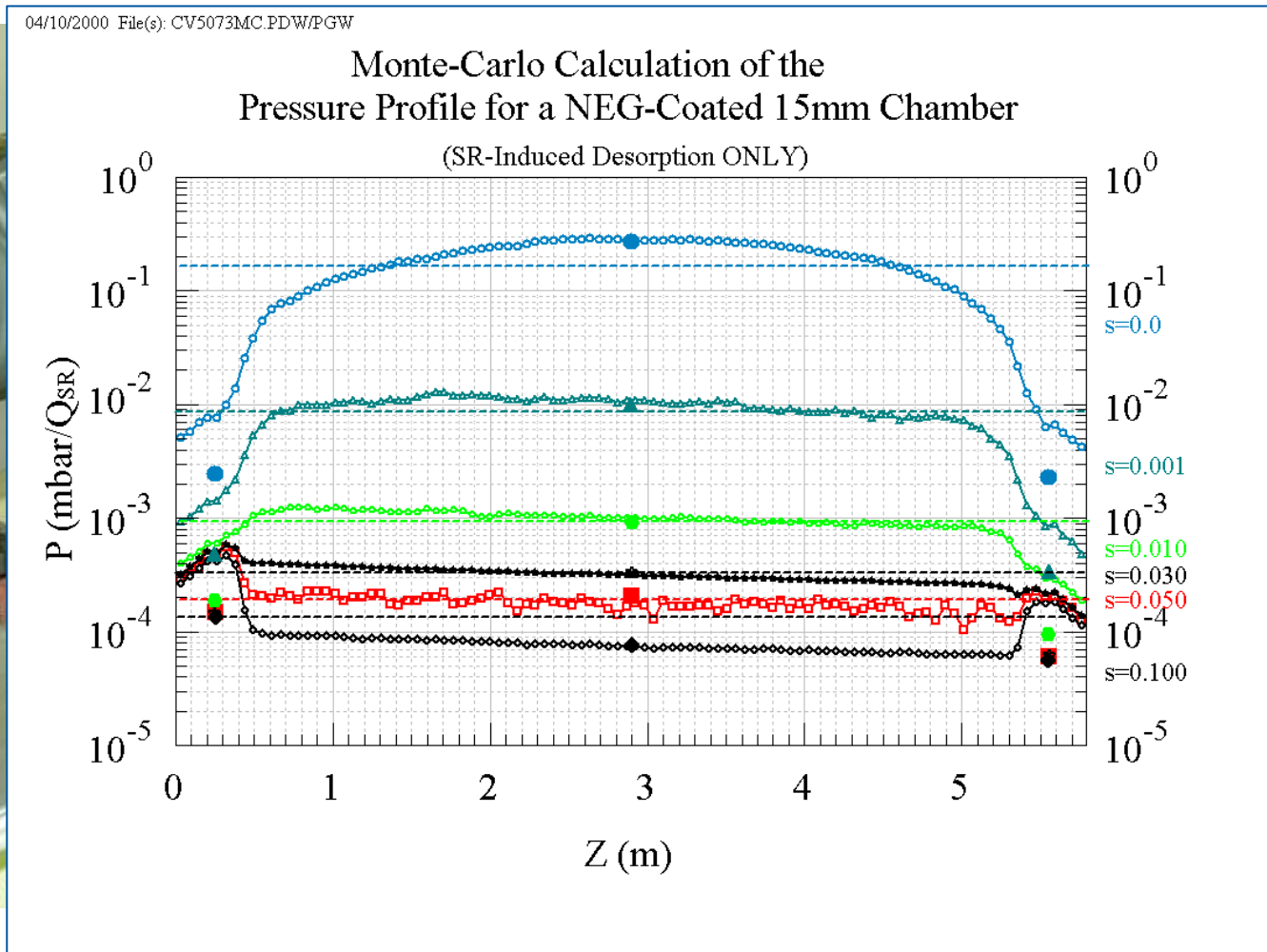
2. TPMC/Molflow+ calculation of the specific conductance of the CLIC quadrupole cross-section (method 2); Molecules are generated on all solid surfaces, pumped at entrance and exit (sticking=0.5); Fit to analytical "parabolic model" pressure profile gives the specific conductance in (l/s/cm²), by taking $\frac{1}{2}$ of the reciprocal of the second order coefficient of the fit, and dividing by length in meters: $C_{spec} = 2.591$ (l·m/s) (~ 1.4% smaller than value obtained with method 1)



3. The LHCb experimental chamber has a conical shape with ID going from 50 to 260 mm, and it is made out of thin (and expensive!) beryllium (courtesy M.A.Galilee)



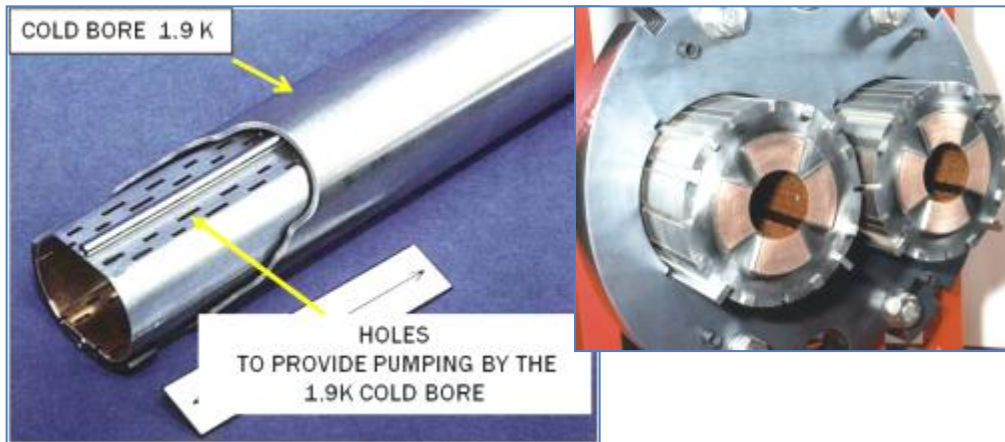
4. The insertion device (ID) vacuum chambers of the ESRF light source have an elliptical cross-section of $57 \times 8 \text{ mm}^2$ (HxV) axis, made out of extruded aluminium (seen here with other extrusions)



5. LHC SC dipole arc sections: 1.9K cold bore with inserted 5-20K beam screen with pumping slots. Material is stainless steel, with co-laminated copper coating on the inside and sawtooth SR absorber

LHC "beam screen":

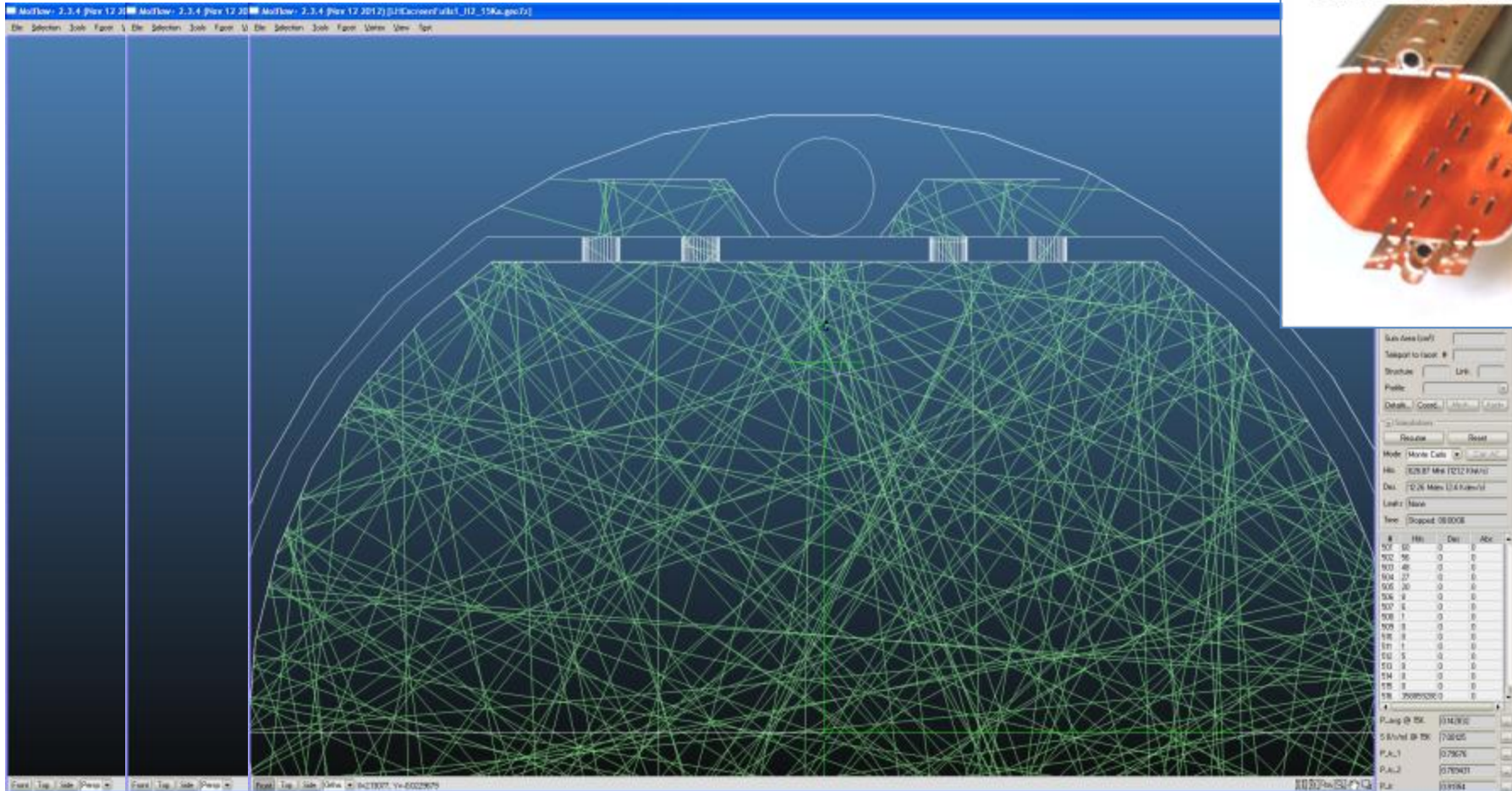
Linear power density: 14 mW/m @ 3.5 TeV
222 mW/m @ 7.0 TeV



BEAM SCREEN AT 5→20 K
USING 2 COOLING CHANNELS



5. LHC SC dipole arc sections: 1.9K cold bore with inserted 5-20K beam screen with pumping slots. Note the uneven adsorption profile on the cold-bore (sticking=1)



4. Conclusions

- The design of an accelerator's vacuum system proceeds in steps & loops:
 - a) Get required base pressure from machine physicists (and/or experiments)
 - b) Define physical and functional interfaces with other subsystems influencing vacuum (magnets, RF devices, beam instrumentation, machine optics, etc...)
 - c) Identify all possible mechanisms and sources of outgassing
 - d) Draft the cross-section of the "best" vacuum chamber profile, in terms of conductances and pumping speeds
 - e) Create or modify the model of the vacuum system
 - f) Run simulations and get pressure profiles
 - g) IF average (and/or local) pressure satisfy physics requirement...
THEN proceed with initial CAD integration work
ELSE go back to b) and loop
 - g) Choose materials, fabrication procedures, vendors compatible with budget (if *too_expensive* you may need to *go back to c*!)
 - h) Ready to start prototyping: IF OK proceed ELSE go back to g)
 - i) Fabrication (validation, testing, etc...)
 - j) Installation
 - k) Commissioning
 - l) Operation

5. References (other than those already mentioned previously)

- CAS Vacuum Schools, 1999 and 2006:
 - <http://cds.cern.ch/record/923393?ln=en> p.285
 - <http://cds.cern.ch/record/402784?ln=en> p.127
- JUAS 2012 presentations by P. Chiggiato and R. Kersevan
- "Introduction to MOLFLOW+ New graphical processing unit-based montecarlo code... ", JVST A27 (2009) no.4 p1017-1023
- M. Ady: Molflow+ web server at CERN:
<http://test-molflow.web.cern.ch/>
- "Monte Carlo simulation of the pressure and f the effective pumping speed in the LEP collider", JM Laurent, T Xu, O Groebner - CERN-LEP-VA 86-02
- United State Particle Accelerator School, "*Vacuum Science and Technology for Accelerator Vacuum Systems*", Jan 2013, Duke University, Y. Li, X. Liu
http://uspas.fnal.gov/materials/13Duke/Duke_VacuumScience.shtml